J|A|C|S ARTICLES

Published on Web 06/28/2010

Transmission Electron Microscopy Evidence of Spontaneous B-Cation Layered Distribution in $NaNb_{1-x}Ta_xO_3$

Almudena Torres-Pardo,[†] Frank Krumeich,[‡] José M. González-Calbet,[†] and Ester García-González*,[†]

Departamento de Química Inorgánica, Facultad de Químicas, Universidad Complutense de Madrid, 28040 Madrid, Spain, and Laboratory of Inorganic Chemistry, ETH Zurich, CH-8093 Zurich, Switzerland

Received April 15, 2010; E-mail: esterg@quim.ucm.es

Abstract: A transmission electron microscopy (TEM) study of the complex $NaNb_{1-x}Ta_xO_3$ ($0.4 \leq x \leq 0.6$) perovskites, combining high-resolution TEM and high-angle annular dark-field scanning TEM, has revealed the formation of extended areas on the crystals where niobium and tantalum order into layers in a 1:1 ratio. $NaNb_{1-x}Ta_xO_3$ oxides are stoichiometric, and there is neither charge difference nor significant ionic size discrepancy between Nb(V) and Ta(V) cations. As d^0 octahedrally coordinated cations, they show a propensity to second-order Jahn−Teller distortion. This distortion, however, manifests itself to different extents for the two cations and is considered the driving force for the layered ordered distribution observed. The niobium−tantalum segregation we have found can also be interpreted as a naturally occurring nanometer-scale phase separation. Albeit occurring in wide regions of the crystals and not in the entire grains, it shows a clear trend toward a long-range ordered disposition. This is reminiscent of the more general behavior of a recently documented class of perovskites that suffer spontaneous nanoscale phase separation to form a superlattice.

Introduction

Cation order−disorder plays a key role in the control of the crystal structure and the properties of many complex perovskite-type oxides. Ferroelectric response, electronic or ionic conductivity, and magnetic behavior strongly depend on the degree of order on the A and B sites. In comparison with the relative rareness of A site ordered perovskites, there are numerous examples of B site ordered systems. As a general fact, a B/B′ ordered distribution can be stabilized when two different cations occupying the same site differ in charge, ionic size, and/or coordination environment.[1]

In the field of ferroelectrics, most of the work devoted to lead-free materials deals with perovskite-type solid solutions. These materials show a unique continuous change from ferroelectric to relaxor behavior versus substitution rate,[2] giving materials with excellent piezoelectric response which qualifies them for potential applications.[3,4] In fact, one strategy to create relaxor ferroelectrics involves the chemical substitution of ions to generate random lattice disorder ABO_3 perovskites. Much of this disorder is produced by chemical substitution of ions of oxidation state the same as or different than that of the host. In addition to being an essential feature, lattice disorder is at the origin of local polar clusters of randomly oriented polarization, and their cooperative interaction produces a long-range ferroelectric state.[5]

Anionic vacancies can induce cationic order of differently coordinated B and B′ cations, but high concentrations of oxygen vacancies have an adverse effect on dielectric properties and the use of ferroelectric materials in stoichiometric amounts. In this case, charge or size differences are primary factors affecting the stability of the ordered state. However, issues such as asymmetric coordination environments and covalence are important in these compounds because asymmetry is a requirement to display the desired ferroelectric behavior.

Although in most of the cases cation ordering leads to homogeneous materials, there are several examples in which spontaneous chemical segregation occurs, giving rise to nanostructured materials formed by separated phases in a periodic array. This is the case with the $(Nd_{2/3-x}Li_{3x})TiO_3$ system[6,7] or the $LaNaMgWO_6$ oxide.[8] These self-assembled nanocomposite materials constitute a very promising category, especially when the periodicity can be controlled by varying the chemical composition and this variation affects the final physical properties of the solid. If unique functionalities can be obtained with a layer-by-layer growth of two-dimensional heterostructures,[9] attractive conductivity, dielectric, or magnetic properties could

[†] Universidad Complutense Madrid.
[‡] ETH Zurich.

(1) Davies, P. K.; Wu, H.; Borisevich, A. Y.; Molodetsky, I. E.; Farber, L. *Annu. Rev. Mater. Res.* **2008**, *38*, 369–401, and references therein.
(2) Simon, A.; Ravez, J.; Maglione, M. *J. Phys.: Condens. Matter* **2004**, *16*, 963–970.
(3) Xu, G.; Zhong, Z.; Bing, Y.; Ye, Z.-G.; Shirane, G. *Nat. Mater.* **2006**, *2*, 134–140.
(4) Mani, R.; Achary, S. N.; Chakrabarty, K. R.; Deshpande, S. K.; Joy, J. E.; Nag, A.; Gopalakrishnan, J.; Tyagi, A. K. *Adv. Mater.* **2008**, *20*, 1348–1352.
(5) Samara, G. A. *J. Phys.: Condens. Mater* **2003**, *15*, R367–R411.
(6) Guiton, B. S.; Davies, P. K. *Nat. Mater.* **2007**, *6*, 586–571.
(7) Guiton, B. S.; Davies, P. K. *J. Am. Chem. Soc.* **2008**, *130*, 17168–17173.
(8) García-Martín, S.; Urones-Garrote, E.; Knapp, M. C.; King, G.; Woodward, P. M. *J. Am. Chem. Soc.* **2008**, *130*, 15028–15037.

also be obtained by manipulating self-assembled, compositionally modulated materials.

In our recent investigations, relaxor-type materials derived from $NaNbO_3$ have been obtained by partially substituting Na by Sr.[10] However, progressive introduction of Ta in Nb sites of $NaNbO_3$ leads to the formation of antiferroelectric materials up to a threshold composition at which materials begin to display ferroelectric behavior.[11] In this paper, we have analyzed the crystal chemistry of the complex $NaNb_{1-x}Ta_xO_3$ ($0.4 \leq x \leq 0.6$) perovskite-type oxides. Extended areas on the crystals are observed where niobium and tantalum are ordered into layers. $NaNb_{1-x}Ta_xO_3$ oxides are stoichiometric, and there is neither charge difference nor significant ionic size discrepancy between Nb(V) and Ta(V) cations. As d^0 octahedrally coordinated cations, they show a propensity to second order Jahn−Teller distortion (SOJT). This distortion, however, manifests itself to different extents for the two cations and is associated with bond network stress and lattice strain; therefore, covalence and asymmetry in the oxygen coordination environment are adequate terms to discuss. Nanoscale phase separation is a concept that can be applied to describe this remarkable microstructural feature. As recently pointed out,[12] the discovery of a perfect two-dimensional phase separation at the nanoscale in $(Nd_{2/3-x}Li_{3x})TiO_3$ opens a new perspective on the microstructure of complex perovskites. Two previous examples illustrate this phenomenon,[7,8] and the results we have obtained provide further support.

Experimental Section

Ceramic samples of nominal composition $NaNb_{1-x}Ta_xO_3$ ($0.4 \leq x \leq 0.6$) were obtained by solid-state reaction from stoichiometric amounts of Na_2CO_3 (99.5%, Merck), Nb_2O_5 (99.99%, Aldrich), and Ta_2O_5 (99.99%, Aldrich). After mixing in an agate mortar, powders were heated in platinum crucibles at 1173 K for 12 h to decompose the sodium carbonate. The resulting powders were reground in an agate mortar, pelleted, and heated in air between 1473 and 1523 K for 48 h, depending on the desired final composition of the material. Samples were finally cooled to room temperature at a cooling rate of 1.5 K min^{-1}.

Magnetic measurements were performed in a Quantum Design XL-MPMS superconducting quantum interference device magnetometer in order to determine the presence of Nb(IV). At 5 K and 1 T, the detected signal did not indicate the presence of Nb(IV) in the samples.

Room-temperature powder X-ray diffraction (XRD) patterns for all samples were collected on a Panalytical X'PERT PRO ALPHA 1 diffractometer with a Ge (111) primary beam monochromator prealigned for Cu $K\alpha_1$ radiation and equipped with an X'Celerator fast detector.

Samples for transmission electron microscopy (TEM) were ultrasonically dispersed in *n*-butanol and transferred to carbon-coated copper grids. Selected area electron diffraction (SAED) experiments were carried out on a PHILIPS CM20FEG SuperTwin electron microscope. High-resolution transmission electron microscopy (HRTEM) was performed on both a JEOL JEM300FEG and a Tecnai 30F (FEI) electron microscope working at 300 kV. Scanning transmission electron microscopy (STEM) was performed on a Tecnai 30F transmission electron microscope (FEI; SuperTwin lens with Cs = 1.2 mm) operating at 300 kV. STEM images were recorded with a high-angle annular dark-field (HAADF) detector (image size, 1024 × 1024 pixels; scan times, 5−20 s; camera length, 200 mm) that almost exclusively detects incoherently scattered electrons (Rutherford scattering), resulting in atomic number (*Z*) contrast.

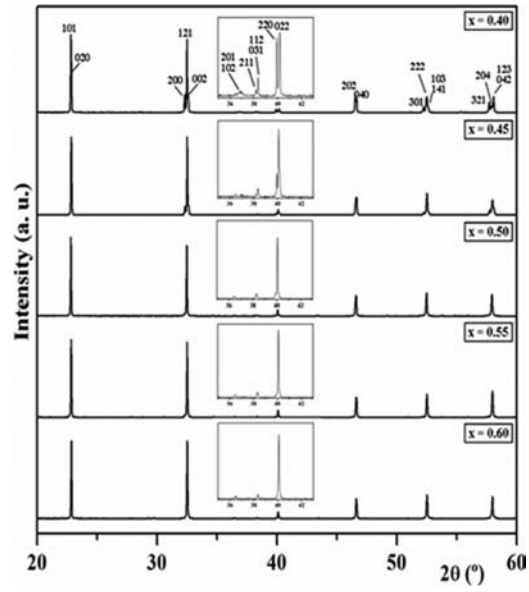

Figure 1. Room-temperature powder XRD patterns corresponding to the $x = 0.4$, 0.45, 0.5, 0.55, and 0.6 compositions of the $NaNb_{1-x}Ta_xO_3$ system. Miller indices refer to the $\sqrt{2}a_c \times 2a_c \times \sqrt{2}a_c$ unit cell.

Crystal-by-crystal chemical microanalysis was performed by energy-dispersive X-ray spectroscopy (EDXS), carried out on a JEOL JEM300FEG microscope equipped with an ISIS 300 X-ray microanalysis system (Oxford Instruments) and a LINK Pentafet EDXS detector. The average cationic composition of the samples was determined on a JEOL 8900 Super Probe electron probe microanalyzer with five wavelength-dispersive X-ray spectrometers operating at 20 kV and 50 μA.

Results

The average cationic composition of all the samples $NaNb_{1-x}Ta_xO_3$ ($0.4 \leq x \leq 0.6$) was confirmed as the nominal composition by means of wavelength-dispersive X-ray spectroscopy (WDS). The results can be found in the Supporting Information. Crystal-by-crystal microanalysis by EDXS showed a Nb:Ta ratio always in agreement with the corresponding nominal composition. Sodium was present in all the crystals, but its content was not quantified by this technique.

The room-temperature powder XRD patterns corresponding to the $NaNb_{1-x}Ta_xO_3$ ($0.4 \leq x \leq 0.6$) oxides are characteristic of a perovskite-type structure (Figure 1). The presence of diffraction maxima around 36 and 38° (2θ) led us to index all the diffractograms on the basis of an orthorhombically distorted $\sqrt{2}a_c \times 2a_c \times \sqrt{2}a_c$ cell (where a_c refers to the cell parameter of the cubic perovskite), and a significant decrease of the splitting of the diffraction maxima is observed as the tantalum content increases.

The structure of the samples was further analyzed by TEM. The results were in agreement with the $\sqrt{2}a_c \times 2a_c \times \sqrt{2}a_c$ unit cell, but some additional features were observed.

Figure 2a corresponds to the SAED pattern of a crystal of $NaNb_{0.4}Ta_{0.6}O_3$ composition. Besides the main reflections of the basic perovskite cell, maxima of lower intensity at $(h/2\ 0\ k/2)_c$ can be observed which indicate the formation of an orthorhombic unit cell with parameters $a \approx c \approx \sqrt{2}a_c$. In addition, diffraction maxima doubling $[100]_c$ and $[001]_c$ (pointed out by

(9) Bousquet, E.; Dawber, M.; Stucki, N.; Lichtensteiger, C.; Hermet, P.; Gariglio, S.; Triscone, J. M.; Ghosez, P. *Nature* **2008**, *452*, 732–736.
(10) Torres-Pardo, A.; Jiménez, R.; González-Calbet, J. M.; García-González, E. *Chem. Mater.* **2009**, *21*, 2193–2200.
(11) Iwasaki, H. *Rev. Electr. Commun. Lab.* **1964**, *12*, 469–487.
(12) Woodward, P. M. *Nat. Mater.* **2007**, *6*, 549–551.

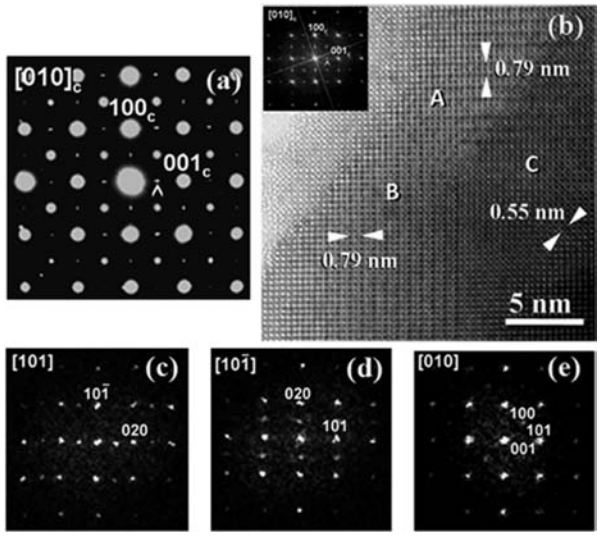

Figure 2. (a) SAED pattern of a crystal of $NaNb_{0.4}Ta_{0.6}O_3$ along the $[010]_c$ projection. Arrows show diffraction maxima corresponding to the two-fold superstructure oriented in two perpendicular directions. Miller indices refer to the cubic perovskite subcell. (b) Corresponding high-resolution electron micrograph. Structural domains of the three different perpendicular orientations of the $\sqrt{2}a_c \times 2a_c \times \sqrt{2}a_c$ unit cell are observed (labeled as A, B, and C). Fourier transforms correspond to (c) area A, (d) area B, and (e) area C. In panels c−e, Miller indices refer to the $\sqrt{2}a_c \times 2a_c \times \sqrt{2}a_c$ unit cell.

an arrow) are observed. These extra spots are consistent with the formation of a two-fold superstructure along the third axis of the orthorhombic cell and suggest the presence of perpendicular domains. The above interpretation is confirmed when observing the corresponding HRTEM image shown in Figure 2b. Distances of 0.79 and 0.55 nm can be easily identified, showing that the crystal is composed of structural domains (labeled A, B, and C) of a $\sqrt{2}a_c \times 2a_c \times \sqrt{2}a_c$ crystal phase oriented in the three perpendicular directions. In this sense, the whole diffraction pattern can be interpreted as the overlapping of the [010], [101], and [10$\bar{1}$] reciprocal lattice projections (Figures 2c,d,e, respectively) of a unit cell $\sqrt{2}a_c \times 2a_c \times \sqrt{2}a_c$.

The systematic study performed on all the samples in the $0.4 \leq x \leq 0.6$ composition range did not reveal any significant change, and crystals were always formed by three-dimensional domains with the metric $\sqrt{2}a_c \times 2a_c \times \sqrt{2}a_c$. In addition to the described structural domains, the microstructural characterization performed by HRTEM has shown, in the entire interval of composition investigated, the presence of extensive defects characterized by the breakdown of long-range order $\sqrt{2}a_c \times 2a_c \times \sqrt{2}a_c$.

Figure 3a corresponds to the HRTEM image of a crystal ($x = 0.4$) oriented along the [10$\bar{1}$] zone axis. Distances of 0.79 nm between characteristic short rows of bright patches are easily observed which indicate the formation of the two-fold superstructure along the *b* orthorhombic axis. However, long-range order is interrupted along the [101] direction due to the presence of antiphase boundaries (APBs). In this case, the APB consists of a translation by $^1/_2$ [010] (see Figure 3b) that tends to occur every 3−4 unit cells in a quasiperiodic disposition. As a consequence, the corresponding SAED pattern (Figure 3c) points to a modulated structure in which the reflections of the two-fold superstructure along the [101] reciprocal direction split and the extra diffraction maxima are elongated along this direction because of the partially ordered distribution of the APBs.

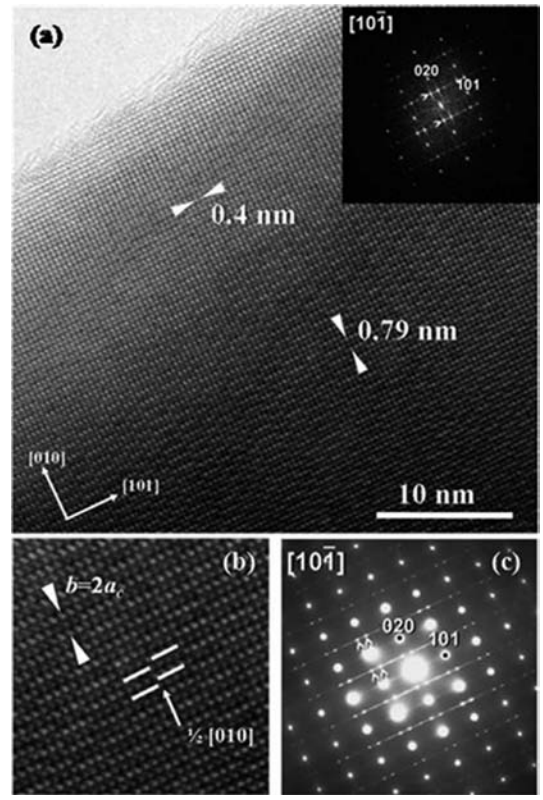

Figure 3. (a) High-resolution electron micrograph of $NaNb_{0.6}Ta_{0.4}O_3$ taken along the [10$\bar{1}$] zone axis. The corresponding Fourier transform is shown in the inset. (b) Enlarged area of (a). Recurrent antiphase boundaries are observed parallel to the [010] direction. (c) Corresponding SAED pattern. The arrows indicate the splitting of the two-fold superstructure diffraction maxima.

Figure 4a shows the SAED diagram of a crystal of $NaNb_{0.4}Ta_{0.6}O_3$ oriented along the [010] zone axis. Streaking between the diffraction maxima indicates, again, structural disorder along the [101] reciprocal direction. The corresponding HRTEM image (Figure 4b) shows distances of 0.55 nm along [100] and [001] of the $\sqrt{2}a_c \times 2a_c \times \sqrt{2}a_c$ unit cell and reveals the presence of dark and bright contrast fringes alternating along the [101] direction. There is no discontinuity in the boundaries between blocks, just a change in the relative intensity of the atomic columns that gives rise to the streaking along the [101] direction. The Fourier transform of the crystal area shown in Figure 4b (inset) depicts discrete diffraction maxima along the [101] reciprocal direction, showing the trend of the defects toward an ordered disposition. It is worth mentioning that, as expected, the trend toward a periodic distribution of defects as well as the extent to which defects occur in the crystals is enhanced after a slow cooling of the sample instead of a quenching from the synthesis temperature.

It is important to note that the microstructural study along the perpendicular [10$\bar{1}$] and [010] projections reveals that the structural defects always occur along the [101] direction, showing in both cases a tendency to be periodic. These facts allow us to consider, as it is explained more deeply in the Discussion section, that the observed dark and bright contrast in Figure 4b could also be related to the presence of APBs along the [101] direction.

The described extended structural defects can be observed in all the crystals of the materials within the $0.4 \leq x \leq 0.6$ interval, and the careful observation performed allowed us to

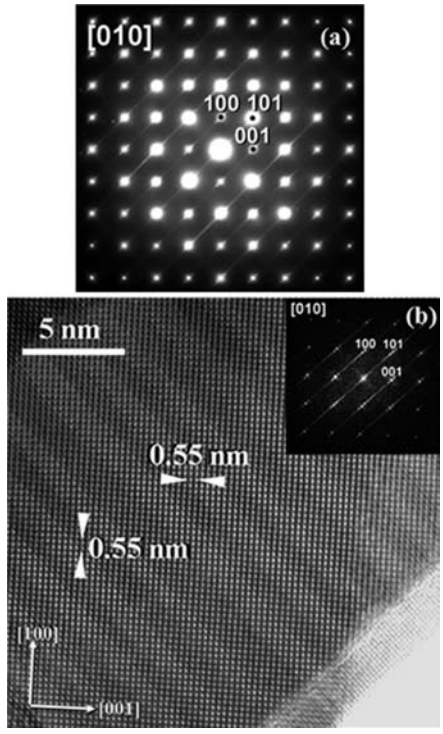

Figure 4. (a) SAED pattern of $NaNb_{0.4}Ta_{0.6}O_3$ taken along the [010] zone axis. Streaking is observed along the [101] reciprocal direction. (b) High-resolution electron micrograph and the corresponding Fourier transform (inset). Discrete extra diffraction spots along [101] are now discernible as a consequence of the quasiperiodic distribution of the stripes in this area of the crystal.

estimate that around 20−25% of the volume of the crystals corresponds to regions with defects. The fact that they appear for chemical compositions close to a Nb/Ta = 1 ratio led us to consider the possibility that they arise as a consequence of a certain ordered distribution of Nb and Ta in the B sublattice of the perovskite structure associated with a fixed Nb/Ta ratio. However, the EDXS nanoanalysis performed on crystal areas as small as 2 nm did not show differences in the chemical composition between defect and defect-free areas of the crystals, the chemical composition being always in agreement with the corresponding nominal composition.

In this sense, and in order to determine a possible inhomogeneous distribution of Nb and Ta associated with the appearance of the antiphase boundaries, characterization by means of high-resolution HAADF STEM has been performed. Since this detector uses the electrons scattered at high angles (i.e., Rutherford scattering) for image formation, there is no phase contribution, and the obtained images are very sensitive to the atomic number Z (Z-contrast imaging).[13]

The HRTEM and the HAADF STEM micrographs of the same area of a crystal of $NaNb_{0.45}Ta_{0.55}O_3$ in the $[10\bar{1}]$ projection are shown in Figure 5a,b. In both images it is possible to identify the antiphase boundary planes as well as the alternation in contrast in the (010) planes that gives rise to the two-fold superstructure along the [010] direction. The inset in Figure 5b corresponds to the intensity profile of the line scan along the direction of the two-fold superstructure. A clear periodic alternation of intensity is observed with $2a_c$ (0.79 nm) periodicity. The fact that this difference in contrast is visible in the HAADF STEM image, which is highly sensitive to the atomic number Z, indicates that it has its origin in a preferential distribution of Ta ($Z = 73$) in the brighter (010) planes and Nb ($Z = 41$) in the darker (010) planes. An enlarged area of a HAADF STEM micrograph of a crystal of $NaNb_{0.45}Ta_{0.55}O_3$ in the same $[10\bar{1}]$ projection is shown in Figure 5c, where an alternation of the contrast in the consecutive (010) planes is observed. The same image after background subtraction is shown in Figure 5d in order to eliminate the contrast effects due to thickness differences. In both images there can be seen adjacent blocks 3−4 octahedra wide in antiphase relationship, as shown also by the intensity profile scans performed in two neighboring blocks (Figure 5e).

When observing the defect areas of the crystals in the perpendicular [010] projection, the HRTEM and the corresponding HAADF STEM micrographs show, however, significant differences. Figure 6a corresponds to the HRTEM image of a crystal of $NaNb_{0.5}Ta_{0.5}O_3$. The periodic contrast variation along [101] is easily identified. However, a homogeneous contrast is observed in the HAADF STEM image (Figure 6b), thus indicating that contrast differences observed by HRTEM in the [010] projection are not due to chemical composition divergence (atomic number variation) between adjacent blocks.

At this point, it is important to keep in mind that the observed contrast variation of (010) planes along the $[10\bar{1}]$ projection in the HAADF STEM images coincides with the direction along which the two-fold superstructure of the orthorhombic cell occurs. In this sense, HAADF STEM was also performed in the defect-free areas of the crystals, in order to investigate the possible ordered distribution of niobium and tantalum in the crystal areas where APBs are not present. Figure 7a shows the HRTEM micrograph of one of these areas in the $[10\bar{1}]$ projection of a crystal of $NaNb_{0.4}Ta_{0.6}O_3$ where the two-fold superstructure can be easily identified along [010]. The corresponding HAADF STEM image (Figure 7b) does not give evidence for any regular contrast variation in the [010] direction, as illustrated by the intensity profile of the line scan along the orthorhombic [010] lattice direction (inset in Figure 7b), therefore indicating that Nb and Ta are randomly distributed in the B-type positions of the defect-free regions of the crystals. As a result, the trend toward an ordered distribution of niobium and tantalum in alternate (010) planes seems to be responsible for the appearance of the APBs in the $NaNb_{1-x}Ta_xO_3$ ($0.4 \leq x \leq 0.6$) crystals.

Discussion

An ordered distribution of tantalum and niobium in $NaNb_{1-x}Ta_xO_3$ ($0.4 \leq x \leq 0.6$) samples in alternate (010) planes of the orthorhombically distorted perovskite-type structure has been detected. The microstructural characterization performed by combining HRTEM and HAADF STEM has revealed the presence of extended structural defects in the form of antiphase boundaries associated with the variations in chemical composition observed.

From the structural information obtained, it is possible to figure out a schematic structural model that places all the results in agreement (Figure 8). In such an idealized model, layers of octahedra occupied by tantalum atoms alternate in an orderly manner with layers of octahedra occupied by niobium atoms along [010]; ordering occurs in blocks four octahedra wide which are related one to each other by an antiphase relationship. In this ideal distribution, not all BO_6 groups have the same metal neighbors. In this sense, octahedra 1 and 4 of each block have as next-nearest metal neighbors [3Ta + 3Nb] (i.e., three gray

(13) Pennycook, S. J. *Ultramicroscopy* **1989**, *30*, 58–69.

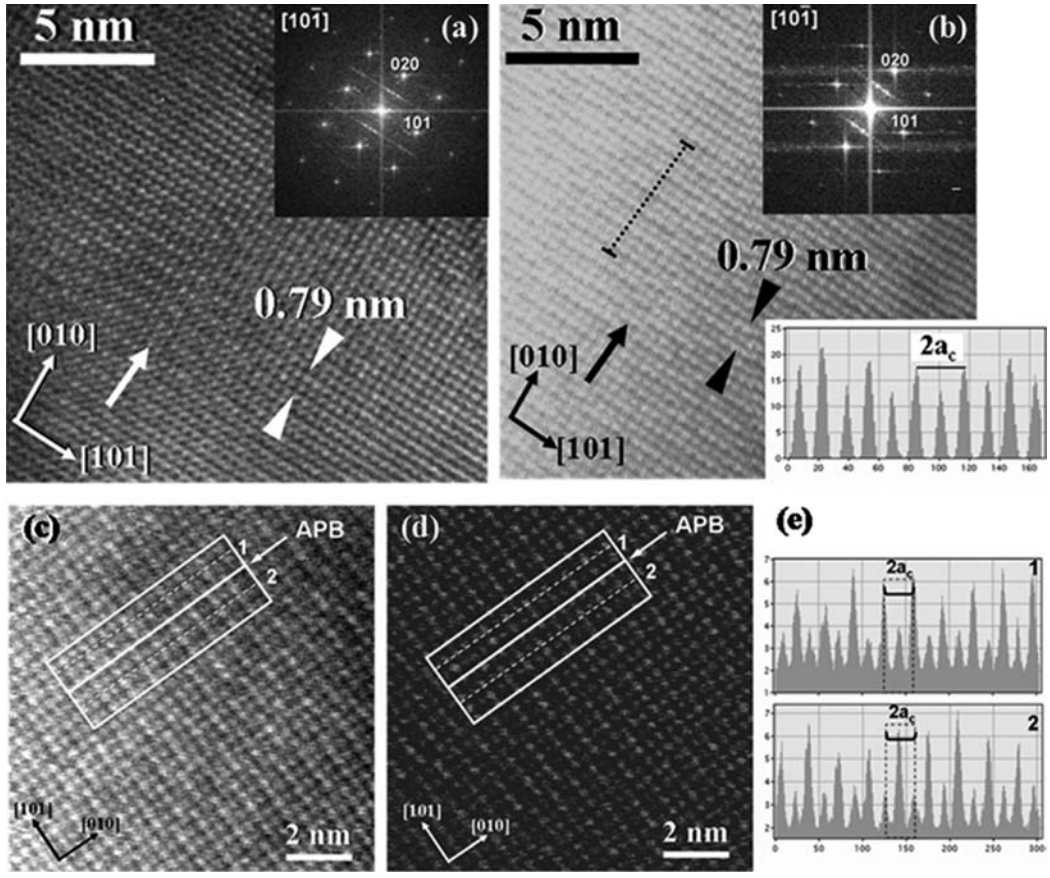

Figure 5. (a) High-resolution electron micrograph and (b) corresponding HAADF image of $NaNb_{0.55}Ta_{0.45}O_3$ taken along the [10$\bar{1}$] zone axis. The arrow allows identification of the same point in both images. Corresponding Fourier transforms are shown in the inset. In (b) the intensity profile corresponding to the dashed line along the [010] direction is shown. (c) Enlarged area of the HAADF image of $NaNb_{0.55}Ta_{0.45}O_3$. (d) Same image after digital background subtraction. In both images, the APB giving rise to two blocks (labeled 1 and 2) is displayed. (e) Intensity profiles of the two consecutive blocks along the [010] direction (dashed white line).

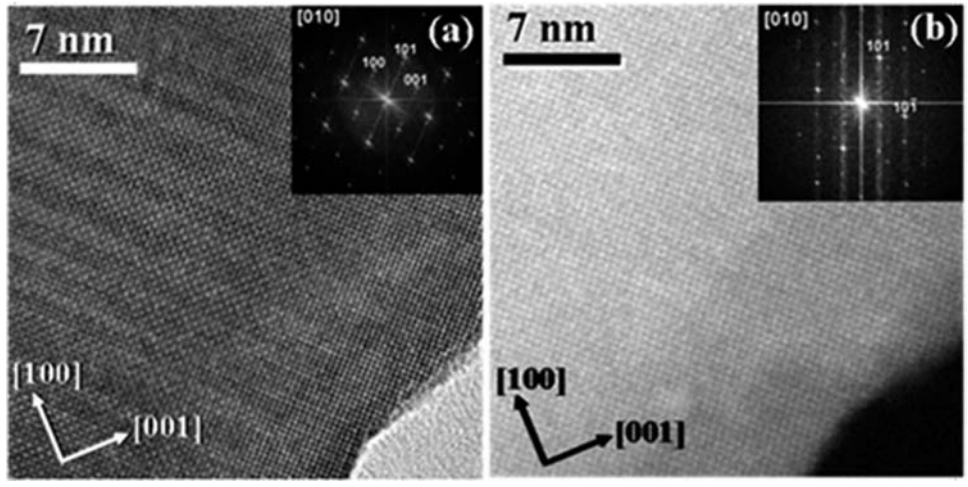

Figure 6. (a) High-resolution electron micrograph and (b) corresponding STEM HAADF image of $NaNb_{0.5}Ta_{0.5}O_3$ taken along the [010] zone axis. Corresponding Fourier transforms are shown as insets.

and three black octahedra), but octahedra 2 and 3 have four metal neighbors of the same nature and two of the opposite, that is to say each Ta has [4Ta + 2Nb] and each Nb has [4Nb + 2Ta]. Assuming that contrast difference has its origin mainly in the chemical composition variation and does not account for crystallographically nonequivalent B sites, the experimental images along the [10$\bar{1}$] projection of the defect areas support this model, although the periodicity between APBs is not as regular as depicted schematically. What is observed is an alternance of 3−4 equivalent dark or bright dots along [101], reflecting the chemical difference, as confirmed when going from the HRTEM to the corresponding HAADF STEM image (see Figure 5a,b). However, in the [010] projection, although the presence of the antiphase boundaries is clearly identified in the HRTEM image through the contrast differences observed along [101] (Figure 6a), the corresponding HAADF STEM

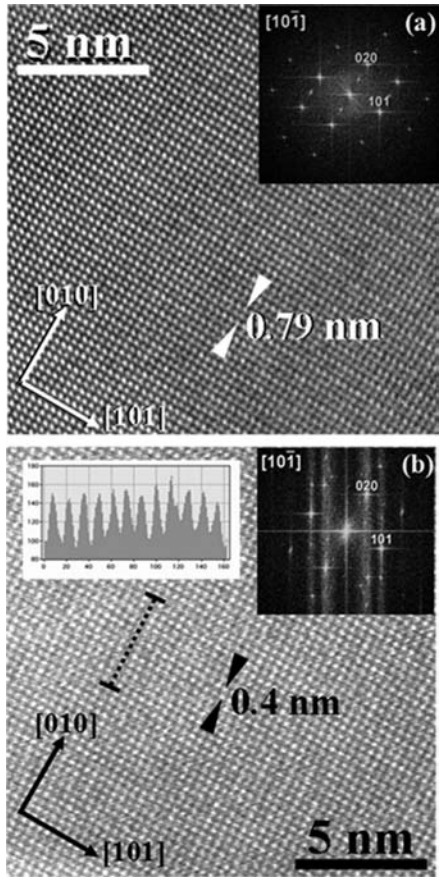

Figure 7. (a) High-resolution electron micrograph and (b) corresponding STEM HAADF image of $NaNb_{0.4}Ta_{0.6}O_3$ taken along the [10$\bar{1}$] zone axis. Fourier transforms are shown in the inset. In (b) the intensity profile corresponding to the dashed line along the [010] direction is shown.

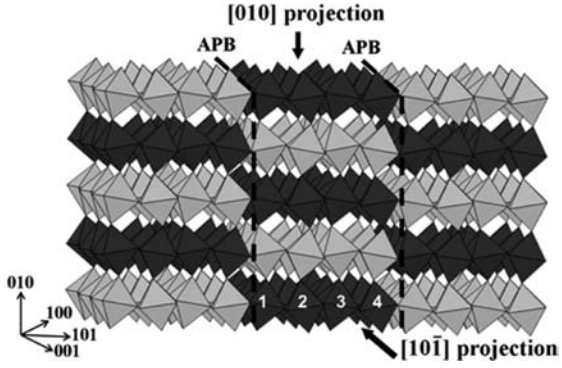

Figure 8. Schematic model of the extended structural defects observed in $NaNb_{1-x}Ta_xO_3$ ($0.4 \leq x \leq 0.6$) by considering an ideal periodic distribution of APBs four octahedra wide. Because information about the octahedral tilting in the defect areas could not be obtained from the refinement of the XRD data, crystallographic data of $NaTaO_3$ from ref 19 have been used as input in order to account for the observed metric of the unit cell.

micrograph does not account for that difference, provided that the average projected potential of the crystal, i.e., the average chemical composition, is constant along this direction, leading to an average intensity of the patches that is similar everywhere (Figure 6b).

At this point it is important to mention that the attempt to quantify the niobium and tantalum content in the (010) planes by acquiring electron energy lost spectra (EELS) and EDXS was unsuccessful. Due to the crystal thickness, a ~0.3 nm diameter for the electron probe size was required to acquire the spectral data sets as line scans along [010]. In this sense, not enough spatial resolution was obtained to determine quantitative chemical composition variations along consecutives (010) planes.

The existence of cationic order at the B site either at short or long range is a recurrent phenomenon in perovskite-type materials.[1] The 1:1 ordered $A_2BB'O_6$ systems are the most common group of ordered B-site perovskites. In this case, the different cations occupy two different sublattices in a "rock salt" disposition, and the result is that B-cations are ordered along the [111] direction with an order vector $^1/_2$[111]. Remarkably, and in contrast to most of the known 1:1 ordered perovskites, La_2CuSnO_6[14] shows a different type of ordering, in which Cu and Sn are arranged in alternating layers along [100]. This rare disposition has also been described for high-pressure Ln_2CuZrO_6 (Ln = Pr, Nd).[15] In La_2CuSnO_6, the CuO_6 polyhedra are strongly Jahn−Teller distorted relative to SnO_6 polyhedra. The authors presumed that the similar size and electronegativity of the cations reduced their tendency to arrange in a rock salt disposition and their chemical dissimilarity and coordination preferences favored the layered distribution against a random arrangement. The superposition of first-order (FOJTJahn−Teller) distortion on octahedron tilting results in the space group $P2_1/m$ and a unit cell metric $a \approx b \approx c \approx 2a_c$.

Asymmetry in the oxide coordination environment is expected in octahedrally coordinated d^0 transition metals. It is well known that cation displacement from the center of a regular octahedron has its origin in a SOJT distortion. SOJT distortion increases when the energy difference between the metal empty d-orbitals and the oxygen filled p-orbitals decreases, which results in mixing of the corresponding metal and oxygen orbitals. Although displacements for a particular B cation are different among the different compounds, they reflect on average the intrinsic distortion preference of each MO_6. The intrinsic preference of a certain cation to distort inside its oxygen polyhedra plays a definite role in ferroelectric perovskites. Out-of-center displacements in over 750 octahedrally coordinated d^0 transition metal oxides have been recently examined using a continuous symmetry measures approach. The magnitudes and directions of the displacements scale roughly with the electronegativity of the cation.[16]

In the same sense, recent studies on the electronic structure of d^0 transition metal oxides in ordered double perovskites and ternary perovskites[17] show that the effective electronegativity of Nb^{5+} is higher than that of Ta^{5+}, and compounds such as $ANbO_3$ and $ATaO_3$ (A = Na, K) illustrate these results. As a consequence, Nb^{5+} is expected to form more covalent bonds with oxygen than Ta^{5+}. Higher covalence is related to a decreasing energy difference between the low-lying d-orbitals and the oxygen 2p-orbitals which, as mentioned, is the origin of the intraoctahedral cationic displacement. In this way, $KTaO_3$ is cubic with regular TaO_6 octahedra and $KNbO_3$ is ferroelectric due to displacements of Nb^{5+} from the center of its octahedron.

(14) Anderson, M. T.; Poeppelmeier, K. R. *Chem. Mater.* **1991**, *3*, 476–482.
(15) Azuma, M.; Kaimori, S.; Takano, M. *Chem. Mater.* **1998**, *10*, 3124–3130.
(16) Ok, K. M.; Halasyamani, P. S.; Casanova, D.; Llunel, M.; Alemany, P.; Alvarez, S. *Chem. Mater.* **2006**, *18*, 3176–3183.
(17) Eng, H. K.; Barnes, P. W.; Auer, B. M.; Woodward, P. M. *J. Solid State Chem.* **2003**, *175*, 94–109.
(19) Ahtee, M.; Darlington, C. N. W. *Acta Crystallogr.* **1980**, *B36*, 1007–1014.

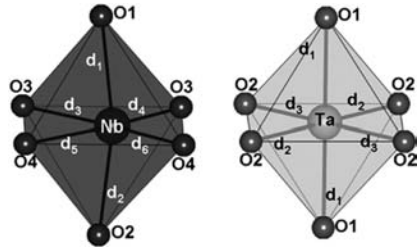

Figure 9. Representation of (a) NbO_6 and (b) TaO_6 octahedra in $NaNbO_3$ and $NaTaO_3$ (from crystallographic data in refs 18 and 19, respectively). Niobium off-center disposition gives rise to six different Nb−O distances ($d_1 = 0.1984$ nm, $d_2 = 0.1999$ nm, $d_3 = 0.2106$ nm, $d_4 = 0.1879$ nm, $d_5 = 0.2129$ nm, and $d_6 = 0.1881$ nm), while TaO_6 octahedra show more regular distances ($d_1 = 0.1965$ nm, $d_2 = 0.1973$ nm, $d_3 = 0.1984$ nm).

In ferroelectric $NaNbO_3$, bond asymmetries result in two short and two long Nb−O bonds in the equatorial plane of the NbO_6 octahedra.[18] This is in strong contrast with the symmetry of Ta−O bonds in TaO_6 octahedra in $NaTaO_6$[19] (see Figure 9). From the above data, it is reasonable to assume a similar trend toward the intraoctahedral distortion in the Nb−Ta compounds considered here, which could act as the driving force for the layered ordered distribution observed for Nb^{5+} and Ta^{5+} cations in the B sublattice. Our experimental data do not allow us to say anything about tilting of the NbO_6 and TaO_6 octahedra, but, in contrast to La_2CuSnO_6, the unit cell metric is $\sqrt{2}a_c \times 2a_c \times \sqrt{2}a_c$.

Terms such as spinodal decomposition, structural intergrowth, or polysomatic order have been found helpful to describe nanostructured materials in the $(Nd_{2/3-x}Li_{3x})TiO_3$ system as a result of nanoscale phase segregation although, as claimed by the authors, none of them account exclusively for the superstructures formed.[6] The niobium−tantalum segregation we have found can be also interpreted as a naturally occurring nanometer-scale phase separation. Although we are far away from the structural characteristics of the above materials, where the nanostructure observed occurs throughout entire grains in all crystals and present periodicities of extraordinary perfection, our findings are reminiscent of them. Undoubtedly, they constitute an important outcome by one side because they represent one of the few examples in which B and B′ cations display layered order, and by the other side because when controlled and ordered throughout the entire crystals may be accompanied by a significant change in the physical properties of the materials.

The compositional modulation generated through the phase segregation (cation segregation) along the [010] direction of the orthorhombically distorted perovskite-type cell can be the origin of a modulation in lattice parameters which must create crystal strain. Therefore, although there are no imaged structural differences between the two phases and the image contrast is mainly the result of the compositional variation of the two phases, there is a structural modulation associated with the quasiperiodic change of chemical composition observed. Lattice and bond network stress because of the interaction between the different MO_6 octahedra can be alleviated by formation of antiphase boundary planes. Energetic considerations must be responsible for the quasiperiodicity in which they appear. In this sense, the investigations performed did not allow us to relate the periodicity in which the APB planes appear with the macroscopic chemical composition of the sample, and the average distance between them is about the same, irrespective of the value of x in $NaNb_{1-x}Ta_xO_3$ ($0.4 \leq x \leq 0.6$).

Efforts are under way to find out the thermodynamic conditions that could lead to a full order situation of the crystals.

Acknowledgment. We acknowledge Prof. K. R. Poeppelmeier for valuable discussions and critical reading of the manuscript. Thanks are also due to Prof. R. Nesper for discussion and general comments. A.T.-P., J.G.-C., and E.G.-G. thank DGICYT (Spain) for financial support through Project MAT2007-61954. We also thank the Electron Microscopy Centers at ETH Zurich (EMEZ) and at UCM (Luis Bru) and the X-Ray Diffraction Center at UCM for facilities.

Supporting Information Available: Table S1, showing average cationic composition of the samples $NaNb_{1-x}Ta_xO_3$ ($0.4 \leq x \leq 0.6$) obtained by means of wavelength-dispersive X-ray spectroscopy. This material is available free of charge via the Internet at http://pubs.acs.org.

JA1031858

(18) Shuvaeva, A.; Antipin, M. Yu.; Lindeman, S. V.; Fesenko, O. E.; Smotrakov, V. G.; Struchkov, Yu. T. *Ferroelectrics* **1993**, *141*, 307–311.